CHAPTER 7

X-RAY NOVA MUSCAE 1991 (=GS 1124-68, GU Mus)

And I'm hovering like a fly,
waiting for the windshield on the freeway...
(Genesis 1974b)

7.1. THE STORY SO FAR

GS 1124-68 (=X-Ray Nova Muscae 1991) was discovered as a bright transient X-ray source on January 8, 1991 by the Ginga (Makino 1991) and the GRANAT (Lund & Brandt 1991) satellites. The analysis of its X-ray spectrum during the outburst (Kitamoto et al. 1992, Grebenev et al. 1992, Ebisawa et al. 1994) showed the presence of a soft component with temperature $kT = 0.96 \pm 0.01$ keV (Greiner et al. 1994) and a hard X-ray power-law tail with spectral index $\alpha = 2.3$ - 2.7; this rapidly allowed the classification of this object as a SXT.

Its optical counterpart, GU Mus, was discovered by Della Valle et al. (1991) one week later, on January 15, 1991. GU Mus increased its luminosity from V~20.5 to V~13.5 at maximum, thus showing a brightening of ~7 magnitudes which is typical of X-ray Novae (van Paradijs & McClintock 1995).

The optical spectrum at maximum (Della Valle et al. 1991), in Fig. 7.1, showed Balmer, He I, He II, N II and N III emission features superimposed on a blue optical continuum, thus resembling the spectra of outbursting CVs. The analysis of the interstellar absorption lines allowed these authors determining an $E(B\text{-}V)$ color excess of 0.3 mag for this system, later confirmed by UV spectroscopic observations (Cheng et al. 1992).

In addition, Ball et al. (1995) detected a transient radio emission during light maximum from X-ray Nova, which is another typical feature of outbursting SXTs.

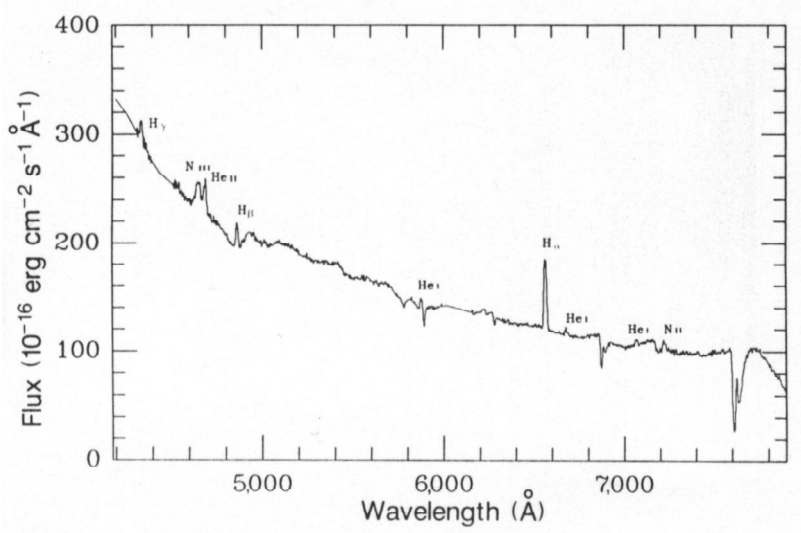

Fig. 7.1. Optical spectrum of GU Mus acquired on January 15, 1991 (from: Della Valle et al. 1991).

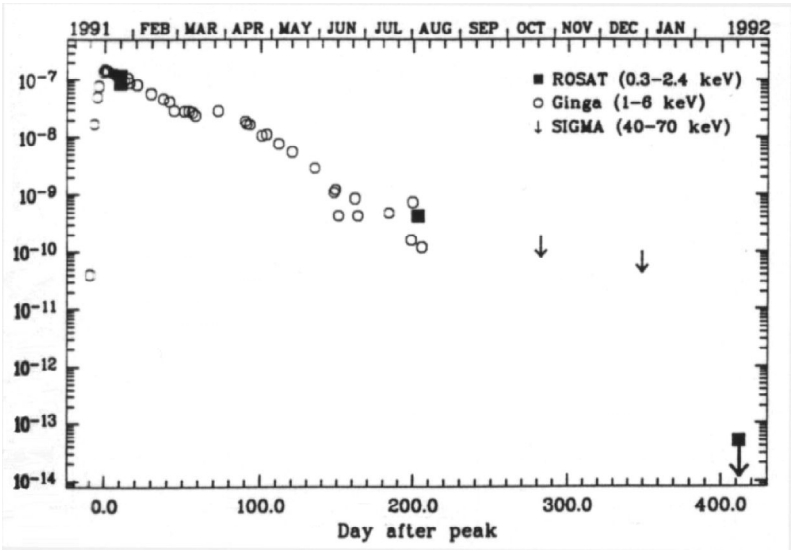

Fig. 7.2. X-ray light curve of GS 1124-68 (=X-ray Nova Muscae 1991). Different symbols correspond to observations made with different satellites. Note the secondary maxima at ~70 and ~200 days after the main X-ray maximum. Fluxes are in units of erg s^{-1} cm^{-2} (from: Greiner et al. 1994).

X-ray and optical observations during the decay showed three important features. The first one is the presence of an e^--e^+ annihilation line in emission at 0.511 MeV (Sunyaev et al. 1992, Goldwurm et al. 1992), which is considered one of the strongest clues of the presence of a BH in a binary system (see the review by Tanaka & Lewin 1995; see also Ch. 3 of this Thesis). The second is the detection of superhumps in the optical light curve between April and June 1991 (Bailyn 1992). The third is that the

X-ray light curve showed two secondary maxima placed ~70 (Kitamoto et al. 1992) and ~200 days (Ebisawa et al. 1994) after the main X-ray peak (Fig. 7.2). On the contrary, until now there is no indication of optical secondary maxima or minioutbursts similar to those displayed by V518 Per (Chevalier & Ilovaisky 1995) and MM Vel (Bailyn & Orosz 1995).

GU Mus reverted to quiescence about one year after the beginning of the outburst (Della Valle 1992). In April 1992, when the system was well at minimum, Remillard et al. (1992) found from the radial velocity curves of the secondary star, an early K type star, that the mass function of the primary is ~3 $M_{\odot}$, which is already beyond the maximum allowed mass for a NS (Rhodes & Ruffini 1974). This value placed GU Mus amongst the galactic BHCs. Later, Orosz et al. (1996) classified the secondary of this system as a K4 V star and determined the distance to GU Mus to be 5.5 kpc.

Finally, Martín et al. (1996) observed the Li I λ6708 line in absorption in the optical quiescent spectrum of the system. This demonstrates the presence of this chemical element in the atmosphere of the secondary similarly to what was observed in other SXTs such as V616 Mon (Marsh et al. 1994), QZ Vul (Harlaftis et al. 1996), V404 Cyg (Martín et al. 1992), Cen X-4 (Martín et al. 1994) and, perhaps, V518 Per (Filippenko et al. 1995).

GU Mus is one of the most known SXTs and one of the best studied during quiescence, despite its intrinsic faintness. On the contrary, not much is known about its optical spectrophotometric decline to the quiescent state from the outburst peak. This is not unusual for the majority of these objects, particularly for those (as they are the bulk; see Ch. 8) below the celestial equator. Thus, in this Chapter 150 observations (images and spectra) taken during the maximum light and the decline of this X-ray Nova, with particular attention to the January - May 1991 period, will be presented. The behaviour of the light curves and of the spectral lines as a function of time will be studied, and a comparison with the behaviour of other SXTs during their decay to quiescence will be made.

7.2. OBSERVATIONS AND DATA REDUCTUION

All the images and the spectra were taken at La Silla (Chile) by means of several ESO telescopes. Table 7.I gives the complete journal of observations along with dates, telescopes, filters or passbands and exposure times. The upper part of Table 7.I lists the images, while the lower part reports the spectroscopic observations.

131 images (56 in the *B*, 41 in the *V* and 34 in the *R* bands) and 19 spectra (with slit widths varying from 1″ to 2″, giving dispersions between 2.0 and 9.6 Å pixel^{-1}) were globally obtained over a time span of nearly one year (from January 15, 1991 to January 1, 1992). The bulk of the observations is however concentrated within the first three months after the outburst. Standard bias and flat field corrections were performed on each frame.

Images were reduced with *DAOPHOT II* (Stetson 1987) and *ALLSTAR* inside *MIDAS*. The X-ray Nova has been calibrated in *B* and *V* by using the field stars 1, 2 and 3 from Bailyn (1992). The *R* magnitudes of these three stars were then determined, since this author does not report them: this has been possible with the use of Mark A and T Phe sequences (Landolt 1992). The resulting *R* magnitudes of the calibration stars are $R_1 = 13.20 \pm 0.03$, $R_2 = 14.49 \pm 0.03$ and $R_3 = 14.53 \pm 0.03$. With these values, the *R* magnitudes of the X-ray Nova were determined. The typical errors on the magnitudes of the object are 0.05 mag in *B* and 0.03 mag both in *V* and in *R*, with the exception of the last photometry measurement, made on January 1, 1992, because of the faintness of GU Mus, already at quiescence (see Sect. 7.3.1).

The reduction of the spectroscopic material was carried out with the *IRAF* package. Also in this case, He-Ar lamps were used for the wavelength calibration, and the standards Feige 56, EG 76, L970-30, LTT 3218, Hiltner 600, CD-32, Wolf 485A and EG 274 for the flux calibration. The spectra were then corrected for interstellar reddening again with the prescription by Cardelli et al. (1989) and using $E(B-V) = 0.30$ as derived by Della Valle et al. (1991).

Finally, as usual, the observation times have been corrected to heliocentric times of mid-exposure and converted to HJDs.

Table 7.I. Log of the observations presented in this Chapter. The upper part of the Table lists the photometric data, while the spectroscopic observations are reported in the lower part.

Date	Telescope	Filter or passband	Number of frames	Exposure times (in minutes)
		IMAGING		
January 15, 1991	2.2 m., NTT	*B; V; R*	2; 2; 3	0.083; 0.16; 0.25; 0.5
January 16, 1991	2.2 m.	*B; V; R*	1; 1; 2	0.16; 0.33
January 17, 1991	2.2 m.	*B; V; R*	1; 1; 1	0.16; 0.5
January 18, 1991	2.2 m.	*B; V; R*	1; 1; 1	0.25; 0.5
January 19, 1991	2.2 m.	*B; V; R*	1; 1; 1	0.42; 0.66
January 20, 1991	2.2 m.	*B; V; R*	1; 1; 1	0.42; 0.66
January 21, 1991	2.2 m.	*B; V; R*	1; 1; 1	0.42; 0.66
January 22, 1991	2.2 m.	*B; V; R*	1; 1; 1	0.42; 0.66
January 23, 1991	NTT	*B; V; R*	1; 1; 1	0.16; 0.33
January 24, 1991	NTT	*B; V; R*	1; 1; 1	0.2; 0.42
January 29, 1991	2.2 m.	*B; V; R*	15; 1; 1	0.5; 1
February 11, 1991	NTT	*R*	2	0.083; 0.5
February 17, 1991	2.2 m.	*B; V; R*	1; 1; 3	0.16; 0.33
February 18, 1991	2.2 m.	*B; V; R*	2; 2; 3	0.16; 0.33
February 19, 1991	2.2 m.	*B; V; R*	1; 1; 1	0.25; 0.5
February 21, 1991	3.6 m.	*B; V; R*	1; 1; 1	0.13; 0.25
February 24, 1991	Danish	*B; V; R*	3; 1; 2	0.25; 0.33; 0.5; 5; 10
February 28, 1991	NTT	*B; V; R*	2; 1; 1	0.1; 0.15; 0.33
March 1, 1991	NTT	*B; V; R*	1; 1; 1	0.1; 0.33
March 2, 1991	NTT	*B; V; R*	1; 1; 1	0.1; 0.33
March 6, 1991	NTT	*B; V; R*	1; 1; 1	0.1; 0.25
March 12, 1991	Danish	*B; V*	3; 3	0.66; 1.33
March 13, 1991	Danish	*B; V*	2; 2	0.66; 1.33
March 14, 1991	Danish	*B; V*	3; 3	0.66; 1.33
March 16, 1991	Danish	*B; V*	1; 4	0.66; 1.33
March 17, 1991	Danish	*B; V*	2; 2	0.66; 1.33
March 18, 1991	Danish	*B; V*	2; 2	0.66; 1.33
March 25, 1991	NTT	*B; V; R*	1; 1; 1	0.16; 0.5
May 19, 1991	3.6 m.	*B; V; R*	1; 1; 1	0.5; 1.5
January 1, 1992	NTT	*B; V; R*	1; 1; 1	1; 2; 3
		SPECTRA		
January 18, 1991	1.5 m.	*Grat*15; *Grat*17	1; 1	15; 18.3
January 19, 1991	1.5 m.	*Grat*15; *Grat*17	1; 1	25; 40
January 20, 1991	1.5 m.	*Grat*17	1	50
January 23, 1991	NTT	#5	1	10
February 15, 1991	1.5 m.	3750 - 7500 Å	1	20
February 21, 1991	1.5 m.	3500 - 10100 Å	1	15
March 6, 1991	NTT	#2; *Grat*5	1; 1	10; 30
March 21, 1991	2.2 m.	#7	1	30
March 25, 1991	NTT	#5; #6	2; 1	10; 20
May 5, 1991	1.5 m.	*Grat*21	1	20
May 19, 1991	3.6 m.	*B300; R300*	1; 1	10; 15

7.3. DATA ANALYSIS

7.3.1. Photometry

The light curves of GU Mus in *B*, *V* and *R* bands are shown in Fig. 7.3a,b,c, respectively. When more than one measurement in the same band was available during the same night, the mean value has been reported in the Figure. One can see that the slopes of the three light curves are very similar. However, fluctuations are seen in each light curve, with amplitudes up to 0.2 mag. These light variations are erratic in the early decline, and later they appear as small light oscillations with typical timescales of about 10 days (see also Fig. 7.7a).

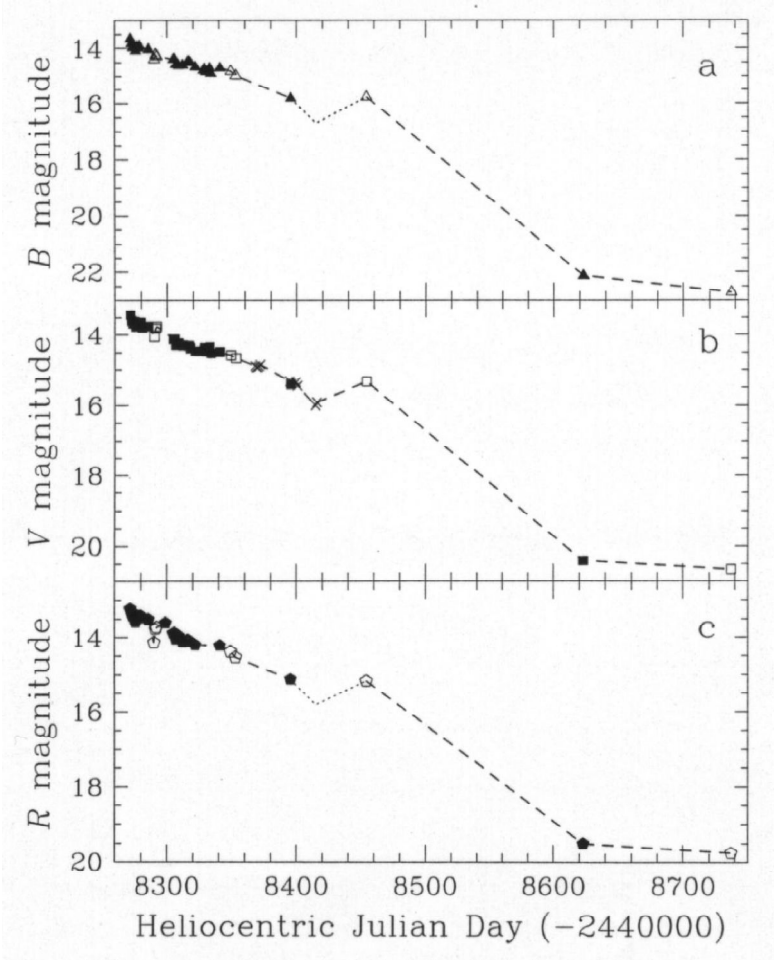

Fig. 7.3a-c. Outburst **a** *B*, **b** *V* and **c** *R* light curves of GU Mus. The decay does not seem to produce strong variations in the light curve slopes seen in the three photometry bands, which are similar although the decline seems to be faster in the *B* band. The possible presence in the *B* and *R* bands of the secondary maximum seen in the *V* light curve ~200 days after the X-ray peak is also indicated with a different hyphenation. Open symbols indicate the *B*, *V* and *R* magnitude determinations made by King et al. (1996a), while crosses correspond to the nightly means of the *V* observations made by Bailyn (1992).

Then, a linear fit to the decay light curves has been performed to estimate the decline rates in the *B*, *V* and *R* bands. Table 7.II reports these decay rates for each photometric band at different decline phases.

Table 7.II. Decay rates (in mag d^{-1}) of the *B*, *V* and *R* outburst light curves of GU Mus computed at different phases of the decline.

Decline phase	*B*	*V*	*R*
January 1991	0.0199	0.0161	0.0135
February - March 1991	0.0109	0.0091	0.0090
April - May 1991	0.0203	0.0168	0.0166
May 1991 - Jan. 1992	0.0278	0.0220	0.0193
Jan. 1991 - Jan. 1992	0.0241	0.0199	0.0178

The three light curves seem to show a *plateau*, or at least a slowing down of the decline, during March 1991, that is, about 70 days after the main X-ray maximum. This behaviour is more evident in the *B* band: two bumps at ~50 and ~70 days after the maximum are clearly visible (see also Fig. 7.7a). The second bump is consistent with the secondary maximum observed in the X-ray band and reported by Kitamoto et al. (1992), while the first one might be associated to a small feature in the X-ray light curve (see Fig. 1, upper panel, of Kitamoto et al. 1992; see also Fig. 7.2). This behaviour is typical of SXTs during the decline (Chen et al. 1993, van Paradijs & McClintock 1995).

The decay starts again in the April-May period, and strengthens in the second part of 1991. It can be also noticed from Table 7.II that, after the initial phase in which the decline is actually the same in the three filters, since March 1991 the decay in the *B* is slightly faster than the ones in *V* and *R*. The same indication comes if one takes into account the whole outburst light curve in the three photometry bands.

However, if one integrates the present photometric data with the magnitude determinations reported by King et al. (1996a) and with the nightly averages of the Bailyn's (1992) observations, one can notice another local maximum in the *V* light curve around HJD 2448460, ~200 days after the X-ray peak: thus, the increased luminosity can be correlated with the tertiary X-ray maximum observed (see Fig. 7.2) by Ebisawa et al. (1994). It is not possible to say whether this phenomenon occurred

also in *B* and *R* light curves, as no observations were made in these bands during that phase; anyway, in Fig. 7.3a,c the possibility of a local maximum also in these two filters has been indicated by means of a different hyphenation.

The presence of optical secondary maxima or minioutbursts during the late decline in other SXTs, such as MM Vel (=X-Ray Nova Velorum 1993; Bailyn & Orosz 1995) and V518 Per (=GRO J0422+32; Chevalier & Ilovaisky 1995, Callanan et al. 1995), would indicate that they are a not unusual feature in these objects, though for these two systems this phenomenon has been purely optical and not associated with a restart of the X-ray activity.

Unfortunately, the lack of observations between the end of July 1991 and January 1992 does not allow the search for the presence of optical minioutbursts such as those seen in the two mentioned SXTs. One can however state that, since the system already reached the quiescent state in January 1992, if ever GU Mus underwent minioutburst episodes, they did not occur after September 1991. This because, as one can see from the optical light curve of V518 Per (Chevalier & Ilovaisky 1995), a minioutburst lasts 20 - 30 days, and the SXT needs few months to reach the quiescent level after having produced the last minioutburst.

The magnitudes of GU Mus at minimum, as measured on January 1, 1992, are B = 22.1 ± 0.3, V = 20.5 ± 0.1 and R = 19.5 ± 0.1, thus in more than acceptable agreement with the mean magnitude determinations by Remillard et al. (1992) and by King et al. (1996a).

The evolution of B-V and V-R colors during the decay is shown in Fig. 7.4a,b, respectively. It is noteworthy that, while the V-R color keeps roughly constant around 0.25 from the beginning of the outburst until mid-May 1991, the B-V seems to decay (0.00118 mag d^{-1}) as the decline proceeds.

The mean B-V color fairly agrees with the value given by Bailyn (1992) for the month of April 1991. One can also note that the object appears to become bluer around HJD 2448320 and ~20-25 days later, that is during the two bumps in the early *B* light curve (see Fig. 7.7a).

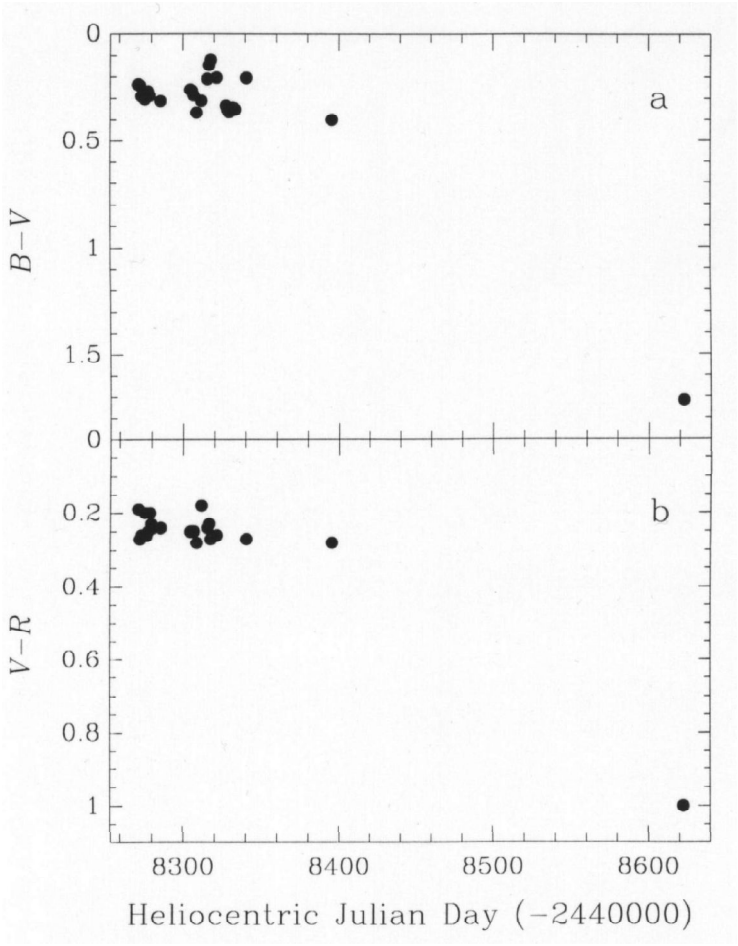

Fig. 7.4. **a** *B-V* e **b** *V-R* color index evolution of GU Mus during the outburst. While *V-R* keeps constant in the first part of the decline, *B-V* undergoes clear variations. In the last decay phase, color indices are back to their original quiescence values.

At the beginning of January 1992, the colors returned to their pre-outburst values (see Della Valle et al. 1991). It is however not possible to know how fast they reached those values because of the mentioned lack of observations of GU Mus in the second half of 1991.

7.3.2. Spectroscopy

The spectra taken during the follow-up period are listed in Table 7.I, lower part, and shown in Figs. 7.5 and 7.6. Fig. 7.5 shows the spectra of the period January-February 1991 with the exception of the spectrum of January 15, 1991, already published by Della Valle et al. (1991) and shown in Fig. 7.1; Fig. 7.6 reports the spectra of the March-May 1991 period.

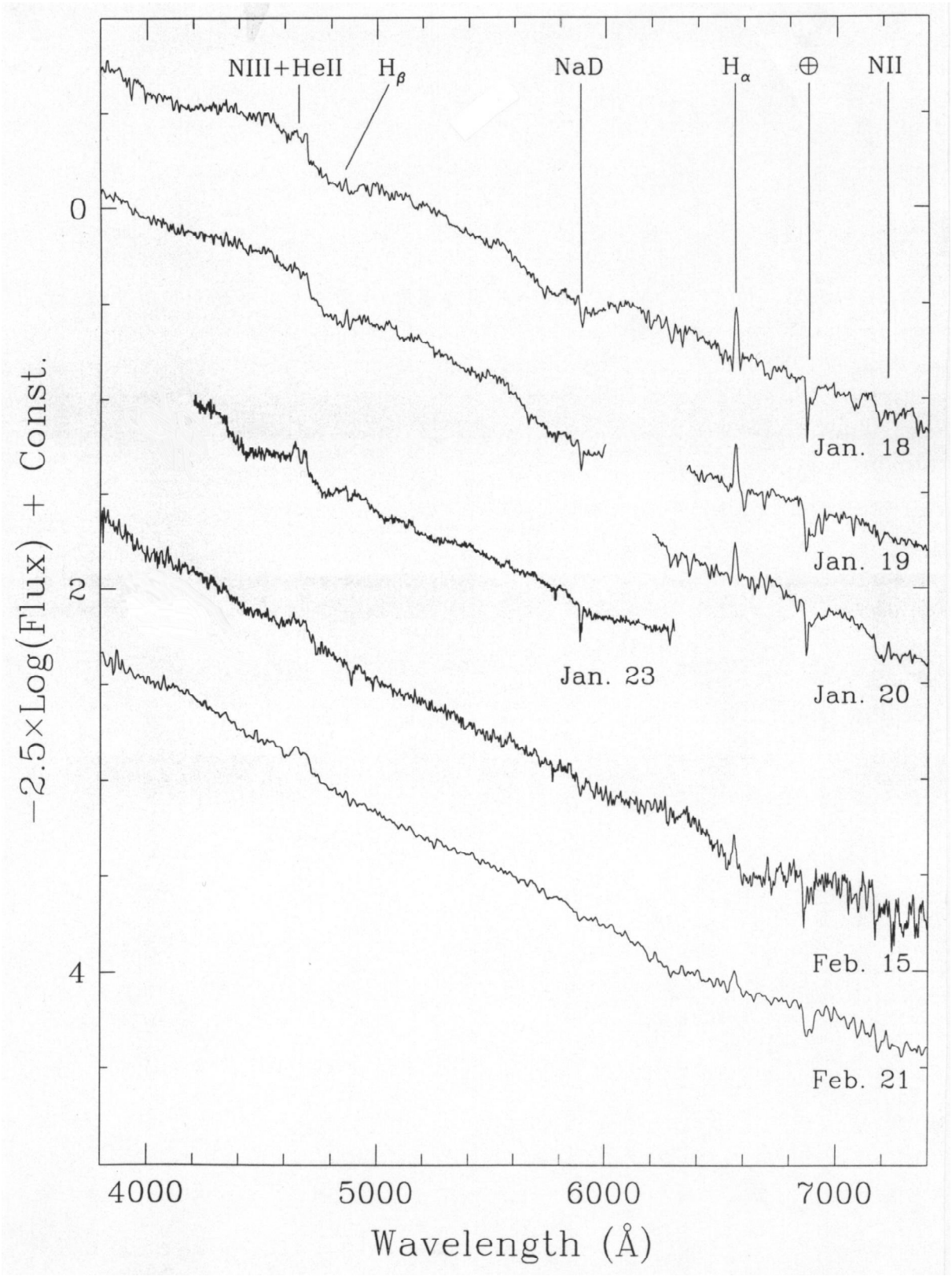

Fig. 7.5. The six spectra of GU Mus acquired between January and February 1991 and listed in Table 7.I. Acquisition dates are reported on the right below each spectrum. The main spectroscopic features are indicated. Fluxes are in erg s^{-1} cm^{-2} $Å^{-1}$. For sake of clarity, the spectra have been separated by 0.5 logarithmic flux units. The additive constant for the spectrum at the top of the Figure is -33.5.

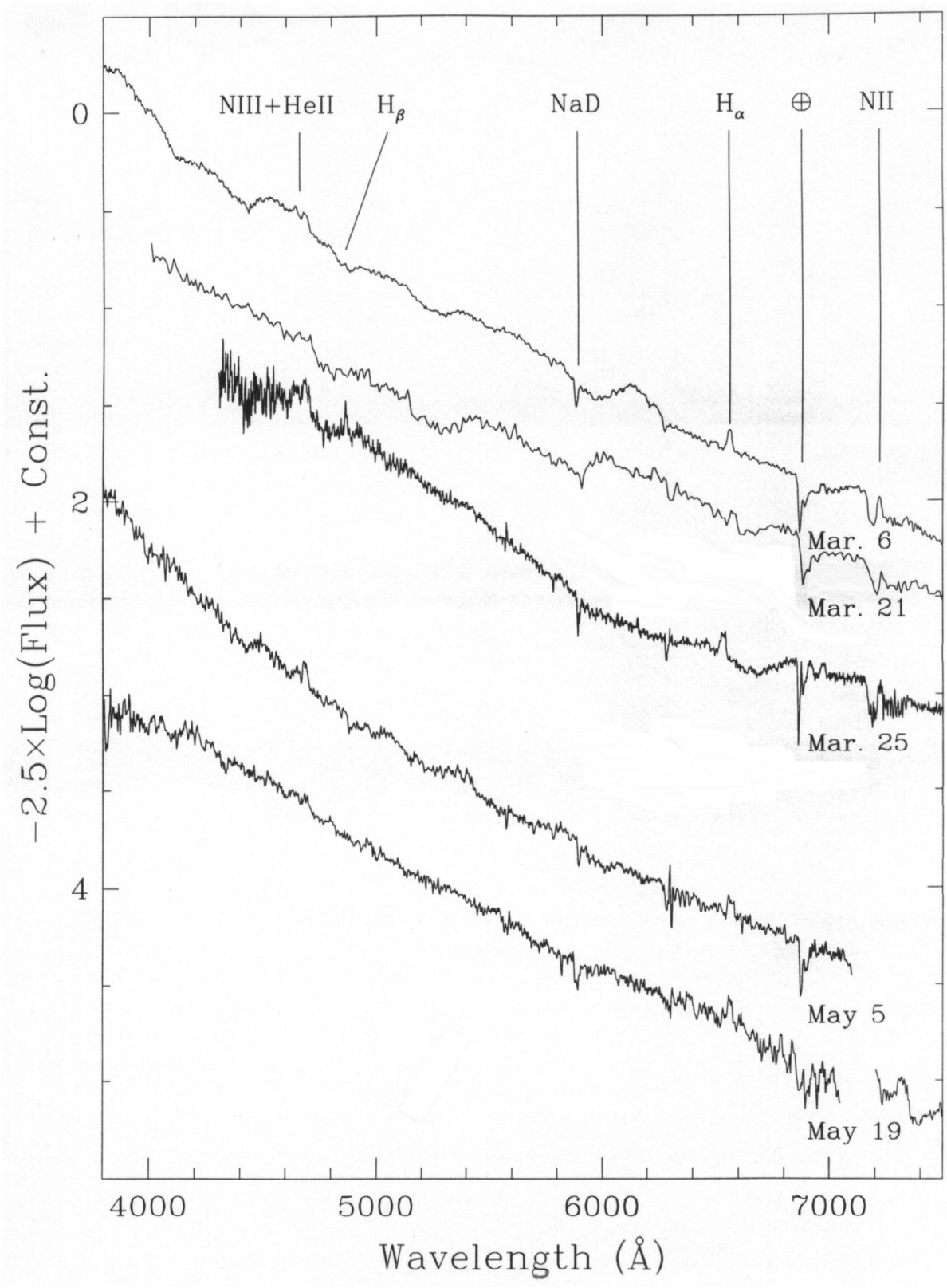

Fig. 7.6. The five spectra of GU Mus acquired between March and May 1991 and listed in Table 7.I. Acquisition dates are reported on the right below each spectrum. The main spectroscopic features are indicated. Fluxes are in erg s^{-1} cm^{-2} $Å^{-1}$. For sake of clarity, the spectra have been separated by 0.5 logarithmic flux units. The additive constant for the spectrum at the top of the figure is -33.5.

As one can see, the most prominent emission lines are H_α, H_β, the N III+He II blend at 4640-4686 Å and, starting from March 1991 (first spectrum from top in Fig. 7.6), the N II λ7220. The only evident absorption lines are the interstellar Na I doublet at 5890 Å and the telluric lines at 6850 Å and 7600 Å (the latter has not been included in the figures).

The mean value of the EW of the NaD absorption, computed on all spectra, is 1.4 ± 0.1 Å, in good agreement with the estimate by Della Valle et al. (1991). According to the relation (Eq. 3.9) between the EW of Na doublet and the *B-V* color excess given by Barbon et al. (1990), it is confirmed that $E(B\text{-}V) \sim 0.3$ mag (see also Cheng et al. 1992). Moreover, it is found that $(B\text{-}V)_o \sim +1.3$ at quiescence, consistent with the spectral classification by Remillard et al. (1992) and by Orosz et al. (1996).

Figure 7.7 shows the first part of the *B* light curve decline together with EWs and FWHMs of the main emission lines visible in the spectra of Figs. 7.5 and 7.6.

More specifically, Fig. 7.7a shows in detail that the early *B* light curve of GU Mus is characterized by the presence of light fluctuations with amplitudes of about 0.2 mag. Such variations appear to be random in the first phase of the decline, and then seem to become oscillations with a timescale of about 10 days.

In Fig. 7.7b,c are instead reported the temporal evolutions of the EWs and FWHMs of H_α, He II λ4686 and of N III λ4640 emission lines, which are the only lines from the spectra presented here which display a reasonable temporal coverage (see Figs. 7.5 e 7.6).

The spectral evolution of the nova during the decline is mainly characterized by the weakening and the broadening of the H_α emission, as shown in Fig. 7.7b,c. An increase of the FWHMs is actually observed also in the He II λ4686 emission, while the behaviour of the N III λ4640 blend is more uncertain due to the broadened profile and to the bad signal-to-noise ratio (see Fig. 5c).

On February 15, 1991 (fifth spectrum from top in Fig. 7.5) and on March 21, 1991 (second spectrum from top in Fig. 7.6) H_α emission appears to be embedded in a wide shallow absorption. For Balmer lines, this is not unusual in SXTs during the decline phase (see e.g. Callanan et al. 1995, Masetti et al. 1997, Bianchini et al. 1997).

The profile of Hβ close to maximum light shows a shallow absorption filled in by an emission core. During the secondary X-ray maximum (third spectrum from top in Fig. 7.6) only the emission component is evident.

The fluxes of He II and N III λ4640 blend decay monotonically with time but rise up during the X-ray reflare. At that time (see Fig. 7.7b,c) also the EW and FWHM of He II show a "jump".

The N II λ7220 is clearly present only in the March spectra (first three spectra form top in Fig. 7.6), and perhaps in the spectrum of January 20 (third spectrum from top in Fig. 7.5), with an average EW of ~2 Å.

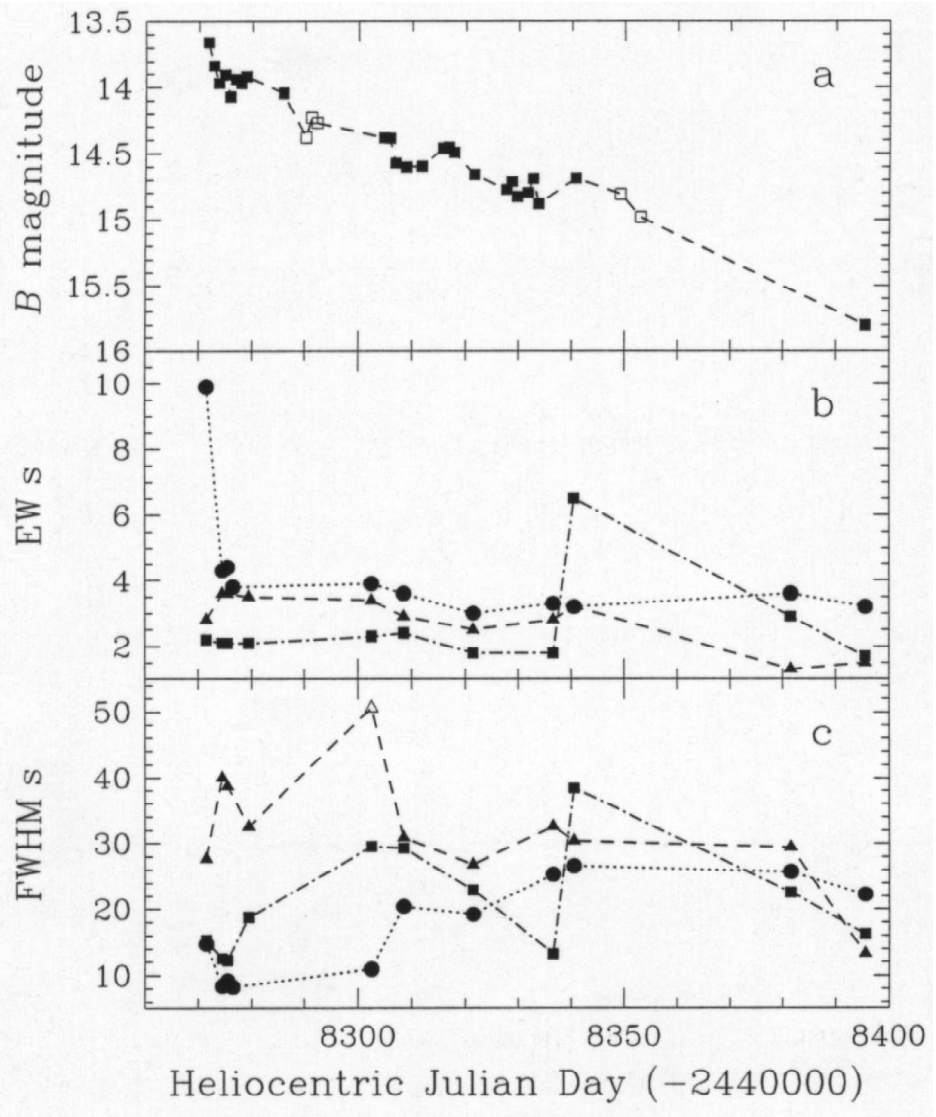

Fig. 7.7a-c. Evolution of the **a** *B* magnitude, **b** EWs and **c** FWHMs of Hα, (circles), He II λ4686 (squares) and N III λ4640 (triangles) between January and May 1991. EWs and FWHMs are both given in Å. The empty triangle in the lower panel corresponds to a rather uncertain measurement, while the open squares in the upper panel indicate the observations of King et al. (1996a).

The continuum seems to become less steep in the blue part as the outburst declines; indeed, the last spectrum of the run (taken on May 19, 1991) appears flatter than the other ones. At this stage, the disk emission is still predominant, as no absorption features of the secondary are seen in that spectum; but this is reasonable since the magnitude of the system was still around $V \sim 15.5$ at the epoch of this observation and the secondary is a K3-K5 dwarf with $V \sim 20.5$ (Orosz et al. 1996).

7.4. DISCUSSION

7.4.1. The light curves

The behaviour of *B*, *V* and *R* light curves seems to follow that of the X-ray emission. Indeed, one can note an increase in the *B*-band luminosity and a variation in the *B*-*V* color index in correspondence of the secondary X-ray maximum occurred ~70 days after the main X-ray peak, and a brightning in the *V* (and possibly also in *B* and *R*) at the time of the tertiary X-ray maximum observed ~200 days after the onset of the outburst. It can be noticed that the optical response of the disk to the X-ray illumination appears more intense when temperature and luminosity of the disk itself are lower, even if in the X-ray band the tertiary maximum is weaker than the secondary maximum.

It is also noteworthy that these minioutbursts are different from those shown by MM Vel (Bailyn & Orosz 1995) and by V518 Per (Chevalier & Ilovaisky 1995) because the latter objects show purely optical reflares well after the end of the X-ray outburst; moreover, the reflares of these two SXTs have no X-ray counterpart. Anyway, the lack of observations in the late decline phase (from July 1991 to January 1992) does not allow stating whether or not GU Mus showed optical minioutburst similar to those displayed by MM Vel e V518 Per: one can only say that (as already made in Sect. 7.3.1), if such optical reflares occurred, they must have appeared not later than September 1991.

Besides this, the poor sampling of the light curves in coincidence of the secondary X-ray maxima (only one point every 2 - 3 days) does not allow saying whether such maxima occurred first in the UV and optical bands and then in the X-rays or viceversa; thus, it is not possible to discriminate whether these phenomena are due to a shift of the inner edge of the disk toward the central compact object or rather to an increase of $\dot{M}$ from the secondary as a response to the increase of X-ray irradiation produced by the main X-ray outburst (see e.g. Chen & Taam 1996 and references therein).

From Table 7.II one can also note that the decay is slower as one moves to higher wavelengths: this may be due to the cooling of the X-ray illuminated zones of the binary system (i.e., the outer disk and the inner face of the secondary).

The light fluctuations observed during the first decline (Fig. 7.7a) might be due to the superhump activity which could have been present also before it was observed in April 1991 by Bailyn (1992). Indeed, superhumps can be observed just after the optical maximum and not only during the decline (Masetti & Regös 1997). Other longer-term light fluctuations, observed during the decline, might be real and correspond to faint secondary maxima. In particular, a sort of 10-day periodicity appears to be present during the decline in the *B* light curve (Fig. 7.7a). According to Warner (1995; see also references therein), this behaviour is similar to that shown by some Classical Novae during the transition phase.

7.4.2. The spectra and the disk stability

During the first five days of the decline the EW of H_α drops quite steeply by a factor 2.5, then it remains at about the same value throughout the first half of 1991 (Fig. 7.7b).

The EW of He II λ4686 emission line shows a bump which approximately starts at HJD 2448340, in coincidence with the secondary maximum of the X-ray (Kitamoto et al. 1992) and the *B* light curves. The increase of luminosity in the high-energy bands (UV and X-rays) should then be responsible for this bump, since the strength of this

emission line is actually correlated with the UV continuum level (Garnett et al. 1991). Later on, the He II line becomes weaker, as also shown by Cheng et al. (1992; their Fig. 3c).

The EW of the N III λ4640 blend appears slightly greater than that of He II before HJD 2448340 and it seems to remain at about the same level throughout the brightening of the He II component. It shows no increase when the X-ray and the *B* light curves have a secondary maximum (see Fig. 7.2, Fig. 7.3 and Fig. 7.7a,b). This behaviour might be explained in the light of the low excitation potential of this line (32 eV, against 50 eV of He II) and from its wide and not well defined profile.

The FWHMs of H_α and of He II emission lines (Fig. 7.7c) tend to increase with time. In particular, that of He II has a maximum in correspondence of the secondary maximum of the X-ray and *B* light curves, thus following the behaviour of the EW of the same line. The FWHM of the N III blend starts with larger values, and then it seems to decrease. The widening at HJD 2448304 (shown in Fig. 7.7c with an empty triangle) is rather uncertain due to the difficult determination of the profile. The FWHMs of He II and N III blend then tend to decrease starting on May 1991. Anyway, the lack of spectroscopic observations after May 19, 1991 does not allow the full confirmation of this trend.

This fact would indicate that, during the decline, the emission region moves inward in the disk, that is, towards larger keplerian velocity radii. One must however note that X-ray Novae may present opposite behaviours in the evolution of optical spectral lines. Some objects, like V518 Per (Shrader et al. 1994) and GRO J1655-40 (Bianchini et al. 1997; see also Ch. 7 of this Thesis), show emission lines with widhts decreasing with time; some other ones, like GU Mus (the present data), V404 Cyg (Gotthelf et al. 1992) and V616 Mon (Whelan et al. 1977) show emission lines which become larger and larger during the decline.

The shrinking of the line width as the luminosity of the object goes down may be explained by the fact that, at light maximum, the external radius of the accretion disk is smaller than at quiescence because of incoming matter with low angular momentum from the X-ray heated secondary. In this way, the disk is not “standard” anymore, and

when the value of $\dot{M}$ from the secondary goes down the outer and cooler part of the disk, in which the lines are formed, can expand again (Bianchini et al. 1997).

In the opposite case, instead, one must assume a rather wide disk also when $\dot{M}$ is high, or when the disk is heavily hit by the X-ray radiation originated in the inner parts of the disk itself. In this way, at light maximum the line-emitting region is placed at larger distances from the central compact object than those expected in the case of lower $\dot{M}$. Actually, the latter is the situation of a "standard" accretion disk, typical of, e.g., a CV (see Ch. 2).

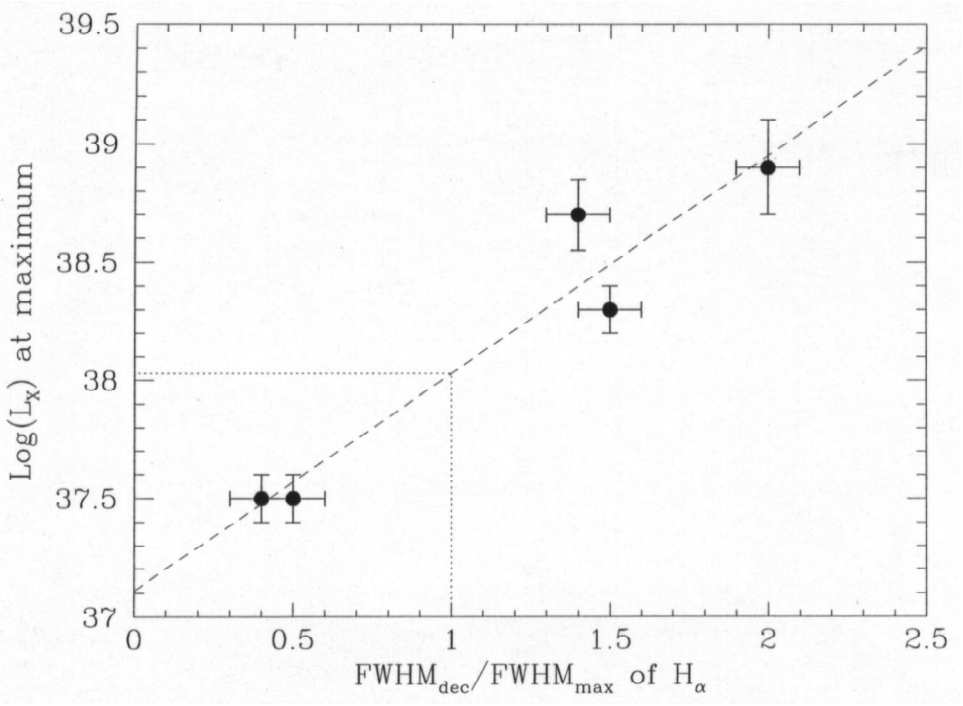

Fig. 7.8. Correlation between the logarithm of the X-ray luminosity (in erg s^{-1}) at maximum and the ratio between the FWHM of Hα emission at mid-decline and that at the beginning of the outburst for 5 SXTs. The long-dashed line represents the least-squares linear fit of the data points.

To investigate this point, in Fig. 7.8 it is plotted the ratio $FWHM_{dec}/FWHM_{max}$ between the FWHMs of the H_α emission line as seen at about 150-200 days after the X-ray peak and at light maximum versus the logarithm of the X-ray luminosity at maximum of the 5 SXTs for which all these quantities are available, i.e. GU Mus (the present data), V404 Cyg (Gotthelf et al. 1992), V616 Mon (Whelan et al. 1977), GRO J1655-40 (Bianchini et al. 1997) and V518 Per (Shrader et al. 1994). The errors on the logarithm of the peak X-ray luminosity are mainly due to the uncertainty on the distance to the objects, while those affecting the FWHM ratios are originated by the

signal-to-noise ratio of the spectra. Both are of the order of 0.1 units. The long-dashed line in Fig. 7.8 represents the weighted least-squares fit of the data points, which is:

$$\mathrm{Log}(L_X) = 0.92\,(\pm 0.15)\frac{FWHM_{\mathrm{dec}}}{FWHM_{\mathrm{max}}} + 37.1\,(\pm 0.2) \qquad (7.1)$$

The correlation coefficient of the data is 0.96, which indicates (admittedly on the basis of a scanty statistic), that these quantities appear to be strongly correlated (see Appendix C of Bevington 1969; see also Sect. 6.3 of this Thesis). Moreover, it can be noted that for X-ray peak luminosities higher than ~10^{38} erg s^{-1} the suggested trend seems to point toward a widening of the H_α line as the outburst declines.

An explanation of this may be the following: higher X-ray luminosities can produce hotter and more viscous disks because of the X-ray irradiation, and thus more stable and relaxed disk structures are formed (King et al. 1996b, van Paradijs 1996). It is also noteworthy that the three SXTs with higher peak X-ray luminosities do not show optical minioutbursts in their late decline or repeated outbursts like those which are instead seen in the two objects with fainter X-ray peaks represented in Fig. 7.8, namely V518 Per e GRO J1655-40. This phenomenon however needs a deeper analysis.

One must also note that, in the cases of V404 Cyg (Casares & Charles 1994) and V616 Mon (Marsh et al. 1994), the mass ratio q in these systems is ~0.06, while in V518 Per (Filippenko et al. 1995) and GRO J1655-40 (Bailyn et al. 1995) this quantity is higher (q > 0.1). For GU Mus, instead, Orosz et al. (1994) and Casares et al. (1996) give the intermediate value of q = 0.13. Thus, it can be hypothesized that, at least in V404 Cyg e V616 Mon, also the tidal effects induced by the secondary on the external edge of the disk act on the value of the ratio between the FWHMs described before: these effects are indeed stronger that in the other systems, thus increasing the viscosity in the outer regions of the accretion disk (Whitehurst & King 1991). This would give an alternative explanation to the existence of rather wide disks during the outburst peak.

REFERENCES OF CHAPTER 7

- Bailyn C.D., 1992, ApJ, 391, 298
- Bailyn C.D., Orosz J.A., 1995, ApJ, 440, L73
- Bailyn C.D., Orosz J.A., McClintock J.E., Remillard R.A., 1995, Nat, 378, 157
- Ball L., Kesteven M.J., Campbell-Wilson D., Turtle A.J., Hjellming R.M., 1995, MNRAS, 273, 722
- Barbon R., Benetti S., Cappellaro E., Rosino L., Turatto M., 1990, A&A, 237, 79
- Bevington P.R., 1969, Data reduction and error analysis for the physical sciences. McGraw-Hill Book Company, New York
- Bianchini A., Della Valle M., Masetti N., Margoni R., 1997, A&A, 321, 477 *(Chapter 4 of this Thesis)*
- Callanan P.J., Garcia M.R., McClintock J.E. et al., 1995, ApJ, 441, 786
- Cardelli J.A., Clayton G.C., Mathis J.S., 1989, ApJ, 345, 245
- Casares J., Charles P.A., 1994, MNRAS, 271, L5
- Casares J., Martín E.L., Charles P.A., Molaro P., Rebolo R., 1996, NewA, 1, 299
- Chen X., Taam R.E., 1996, ApJ, 466, 404
- Cheng F.H., Horne K., Panagia N. et al., 1992, ApJ, 397, 644
- Chevalier C., Ilovaisky S.A., 1995, A&A, 297, 103
- Della Valle M., Jarvis B.J., West R.M., 1991, Nat, 353, 50
- Della Valle M., 1992, ESO Messenger, 67, 35
- Ebisawa K., Ogawa M., Aoki T. et al., 1994, PASJ, 46, 375
- Filippenko A.V., Matheson T., Ho L.C., 1995, ApJ, 455, 614
- Garnett D.R., Kennicutt R.C., Chu Y.-H., Skillman E.D., 1991, ApJ, 373, 458
- Goldwurm A., Ballet J., Cordier B. et al., 1992, ApJ, 389, L79
- Gotthelf E., Halpern J.P., Patterson J., Rich R.M., 1992, AJ, 103, 219
- Grebenev S.A., Sunyaev R.A., Pavlinskij M.N., 1992, SvA Lett., 18, 5
- Greiner J., Hasinger G., Molendi S., Ebisawa K., 1994, A&A, 285, 509
- King N.L., Harrison T.E., McNamara B.J., 1996a, AJ, 111, 1675
- King A.R., Kolb U., Burderi L., 1996b, ApJ, 464, L127
- Kitamoto S., Tsunemi H., Miyamoto S., Hayashida K., 1992, ApJ, 394, 609
- Landolt A.U., 1992, AJ, 104, 340
- Lund N., Brandt S., 1991, IAU Circ. 5161
- Makino F., 1991, IAU Circ. 5161
- Marsh T.R., Robinson E.L., Wood J.H., 1994, MNRAS, 266, 137
- Martín E.L., Rebolo R., Casares J., Charles P.A., 1992, Nat, 358, 129
- Martín E.L., Rebolo R., Casares J., Charles P.A., 1994, ApJ, 435, 791
- Martín E.L., Casares J., Molaro P., Rebolo R., Charles P.A., 1996, NewA, 1, 197
- Masetti N., Regös E., 1997, NewA, 2, 429
- Masetti N., Bianchini A., Della Valle M., 1997, A&A, 317, 769 *(Chapter 5 of this Thesis)*
- Orosz J.A., Bailyn C.D., Remillard R.A., McClintock J.E., Foltz C.B., 1994, ApJ, 436, 848
- Orosz J.A., Bailyn C.D., McClintock J.E., Remillard R.A., 1996, ApJ, 468, 380
- Remillard R.A., McClintock J.E., Bailyn C.D., 1992, ApJ, 399, L145
- Remillard R.A., Orosz J.A., McClintock J.E., Bailyn C.D., 1996, ApJ, 459, 226
- Rhodes C.E., Ruffini R., 1974, Phys. Rev. Lett., 32, 324
- Shrader C.R., Wagner R.M., Hjellming R.M., Han X.H., Starrfield S.G., 1994, ApJ, 434, 698
- Stetson P.B., 1987, PASP, 99, 191
- Sunyaev R.A., Churazov E., Gilfanov M. et al., 1992, ApJ, 389, L75
- Tanaka Y., Lewin W.H.G., 1995, Black-hole binaries. In: X-ray Binaries, Lewin W.H.G., van Paradijs J., van den Heuvel E.P.J. (eds.), Cambridge Univ. Press, Cambridge, p. 126
- van Paradijs J., 1996, ApJ, 464, L139
- van Paradijs J., McClintock J.E., 1995, Optical and ultraviolet observations of X-ray binaries. In: X-ray Binaries, Lewin W.H.G., van Paradijs J., van den Heuvel E.P.J. (eds.), Cambridge Univ. Press, Cambridge, p. 58
- Warner B., 1995, Cataclysmic Variable Stars. Cambridge Univ. Press, Cambridge
- Whelan J.A.J., Ward M.J., Allen D.A. et al., 1977, MNRAS, 180, 657
- Whitehurst R., King A.J., 1991, MNRAS, 249, 25